FLUID DYNAMIC ASPECTS OF THE POROUS WETTED WALL PROTECTION SCHEME FOR IFE REACTORS

S. Shin, F. Abdelall, D. Juric, S. I. Abdel-Khalik, M. Yoda, D. Sadowski, and the ARIES Team

George W. Woodruff School of Mechanical Engineering

Georgia Institute of Technology

Atlanta, GA 30332-0405 USA

Number of Pages: 18

Number of Figures: 13

Number of Tables: 1

---

* Corresponding Author:

Dr. S. I. Abdel-Khalik
School of Mechanical Engineering
Georgia Institute of Technology
771 Ferst Drive
Atlanta, GA 30332-0405

Phone: (404) 894-3719
FAX: (404) 894-8496
E-Mail: said.abdelkhalik@me.gatech.edu

FLUID DYNAMIC ASPECTS OF THE POROUS WETTED WALL PROTECTION SCHEME FOR IFE REACTORS

S. Shin, F. Abdelall, D. Juric, S. I. Abdel-Khalik, M. Yoda, D. Sadowski, and the ARIES Team

ABSTRACT

A numerical and experimental investigation has been conducted to analyze the fluid dynamic aspects of the porous wetted wall protection scheme for IFE reactor first walls. A level contour reconstruction method has been used to track the three-dimensional evolution of the liquid film surface on porous downward-facing walls with different initial film thickness, liquid injection velocity through the porous wall, surface disturbance amplitude, configuration and mode number, liquid properties, and surface inclination angle. Generalized charts for the computed droplet detachment time, detached droplet equivalent diameter, and minimum film thickness during the transient for various design parameters and coolant properties are presented.

An experimental test facility has been designed and constructed to simulate the hydrodynamics of downward-facing porous wetted walls, in order to validate the numerical results over a wide range of parameters. Non-dimensionalization of the model shows that water can be adequately used as a simulant to validate the numerical results. Preliminary experimental results show good agreement with model predictions. The results of this investigation should allow designers of conceptual IFE reactors to identify appropriate "windows" for successful operation of the porous wetted wall protection concept for different coolants.

INTRODUCTION

The energy release from the exploding pellets of inertially confined fusion systems consists of energetic neutrons, photons, and charged particles that eventually dissipate their kinetic energies in the walls surrounding the chamber. Energy deposition by the soft X-rays and charged particles takes place in an extremely thin surface layer, causing rapid surface heating of "unprotected" first walls. These photon and ion irradiations may cause excessive wall erosion, thereby limiting the wall lifetime. Numerous studies of the thermal-mechanical response of IFE reactor first walls for different wall materials, target yields (i.e. wall loadings), repetition rates, and target designs (i.e. spectra) have been reported in the literature (1-8). The results of these studies point to the need for a wall protection scheme to assure wall survival at practical cavity sizes (i.e. wall loadings).

Among the IFE first wall protection schemes is the wetted wall concept, originally proposed by Los Alamos (9-10) and later adopted by other conceptual reactor designs. In the Prometheus-L study (11), a thin film (0.5mm) of liquid lead is allowed to form on the surface of a porous silicon carbide first wall. The X-rays produced by the exploding targets deposit their energy in the film, which prevents surface heating of the silicon carbide first wall. The ionic debris that arrive shortly (a few μs) thereafter deposit their energy either in the lead vapor cloud produced by the X-ray energy deposition or in the remaining liquid film, thereby causing further evaporation. Re-condensation of the vapor allows the energy deposited in the film to be recovered prior to the next target explosion, albeit over a longer time period, thereby limiting first wall heating and thermal stress.

Several studies have been performed to analyze the thermal response of the liquid film to the pulsed photon and ion irradiations, as well as the thermal-mechanical response of the

underlying solid first wall (8, 11-13). Much work has also been reported in the chemical engineering literature on the fluid dynamics and stability of liquid films on vertical and upward facing inclined surfaces (14-18). However, no work has heretofore been reported on the stability of thin liquid films on downward facing solid surfaces with liquid injection through the wall.

Among the critical questions that must be addressed to establish the viability of the wetted wall concept are: (1) Can a stable liquid film be maintained on the upper section of the chamber? (2) Can the film be reestablished over the entire cavity surface prior to the next target explosion? and (3) Can a minimum film thickness be maintained to provide adequate protection during the next target explosion? To this end, a numerical and experimental investigation has been undertaken to examine the hydrodynamics of thin liquid films formed on the downward-facing surface of a porous wall. The aim is to determine the effect of different design and operational parameters (film thickness, liquid injection velocity, inclination angle, liquid properties, and surface disturbance amplitude and configuration) on liquid film stability between explosions. Here, we report the results of a numerical study on the effects of these parameters on the transient, three-dimensional, topology of the film free surface, the frequency of liquid droplet formation and detachment, the size of detached droplets, and the minimum film thickness prior to droplet detachment. An experimental study aimed at verifying the results of the numerical model is described; preliminary experimental results are also presented.

THEORETICAL MODEL

When applied to the downward-facing upper surface of the chamber, the hydrodynamics of the wetted wall protection scheme can be viewed as a variation of the well-known Rayleigh-Taylor instability problem, which occurs when a heavy fluid is situated above a light fluid in a

gravitational field aligned toward the light fluid. Numerous studies of the Rayleigh-Taylor instability problem have been reported in the literature. None of these studies, however, includes a bounding solid wall with continuous injection of the heavier fluid as is the case for the porous wetted wall concept. A detailed review of recent work on the Rayleigh-Taylor instability problem can be found in (19).

In this study, a state-of-the-art level contour reconstruction technique has been developed and used to track the three-dimensional evolution of the liquid film surface on a porous downward-facing wall with different liquid injection velocities and initial film thickness. The technique stems from Tryggvason's finite difference/front tracking method developed for two- and three-dimensional isothermal multi-fluid flows (20-22). Here, the method has been simplified by eliminating logical connectivity, thus eliminating the associated algorithmic burden, while retaining the accuracy and advantages of explicit Lagrangian surface tracking. A primary advantage of this method is its ability to naturally and automatically handle interface merging and breakup in three-dimensional flows. The elements are constructed on a level contour of an existing characteristic indicator function (Heaviside function which takes the value of unity in one fluid and zero in the other fluid). With this level contour reconstruction technique the operations of element deletion, addition and reconnection are accomplished simultaneously in one step and without the need for element connectivity. Furthermore, once the elements are constructed, interface normals and element areas are automatically defined and surface tension forces are accurately computed directly on the interface elements. The approach allows one to compute as much of the interfacial physics as possible directly on the sharp interface before distributing this information to the fixed grid. A more detailed description of the techniques may be found in (19, 23).

One set of transport equations, valid for both fluids, is solved. This local, single field, formulation incorporates the effect of the interface in the equations as delta-function source terms, which act only at the interface. Equations for the material property fields can be written for the entire domain using a Heaviside function which we call the indicator function, $I(\mathbf{x},t)$.

The values of the material property fields at every location can then be given by

$$b(\mathbf{x},t) = b_1 + (b_2 - b_1)I(\mathbf{x},t) \tag{1}$$

where the subscripts 1 and 2 refer to the respective fluids, b stands for either the density ρ, or the viscosity, μ. The indicator function $I(\mathbf{x},t)$ is found by solving the Poisson equation

$$\nabla^2 I = \nabla \cdot \int_{\Gamma(t)} \mathbf{n}\delta(\mathbf{x} - \mathbf{x}_f)\mathrm{d}s \tag{2}$$

Here, $\mathbf{n}$ is the unit normal to the interface, $\mathbf{x}_f = \mathbf{x}(s,t)$ is a parameterization of the interface $\Gamma(t)$, and $\delta(\mathbf{x}-\mathbf{x}_f)$ is a three-dimensional delta function that is non-zero only when $\mathbf{x} = \mathbf{x}_f$. Note that the right hand side of this Poisson equation is a function only of the known interface position, a fact we use to advantage in our numerical implementation. The interface is advected in a Lagrangian fashion by integrating:

$$\frac{\mathrm{d}\mathbf{x}_f}{\mathrm{d}t} \cdot \mathbf{n} = \mathbf{V} \cdot \mathbf{n} \tag{3}$$

where $\mathbf{V}$ is the interface velocity vector. In the absence of phase change, the interface velocity will be equal to the fluid velocity at the interface, $\mathbf{V} = \mathbf{u}_f = \mathbf{u}(\mathbf{x}_f)$.

The momentum equation is written for the entire flow field and the forces due to surface tension are applied as body forces, which act only at the interface. For the confined Rayleigh-

Taylor instability simulation performed here, we assume that there is no mass transfer by phase change at the interface, so that we can forego the need to solve the energy equation and use a single non-dimensional momentum equation for both fluids. Future model enhancements will account for non-isothermal effects, including evaporation and condensation at the interface.

In non-dimensionalizing the governing equations and boundary conditions, we have defined the Laplace length scale $l = (\sigma/g(\rho_L-\rho_G))^{1/2}$, the velocity scale as $U_o = (gl)^{1/2}$, the pressure scale as $P_o = \rho_L U_o^2$, and the time scale as $t_o = l/ U_o$. Here, the subscript "L" refers to the film liquid injected through the porous wall (heavy fluid), while the subscript "G" refers to the low pressure gas (vacuum) within the chamber (light fluid). Thus, the governing non-dimensional momentum equation can be expressed as:

$$\frac{\partial \rho^+ \mathbf{u}}{\partial t} + \nabla \cdot (\rho^+ \mathbf{u}\mathbf{u}) = -\nabla p + \rho^+ \mathbf{g} + \frac{1}{Re}\nabla \cdot \mu^+ (\nabla \mathbf{u} + \nabla \mathbf{u}^{\mathrm{T}}) + \int_A \frac{1}{We}\kappa \vec{\mathbf{n}} \delta(\mathbf{x} - \mathbf{x}_f) dA \qquad (4)$$

where,

$$\frac{\rho_G}{\rho_L} = \rho^*, \ \frac{\mu_G}{\mu_L} = \mu^* \qquad (5)$$

$$\rho^+ \equiv \rho(\mathbf{x},t)/\rho_L = 1 + (\rho^* - 1) I(\mathbf{x},t) \qquad (6)$$

$$\mu^+ \equiv \mu(\mathbf{x},t)/\mu_L = 1 + (\mu^* - 1) I(\mathbf{x},t) \qquad (7)$$

$$Re = \frac{\rho_L U_o l}{\mu_L}, \ We = \frac{\rho_L U_o^2 l}{\sigma} = \frac{\rho_L}{\rho_L - \rho_G} \qquad (8)$$

Here, P is the pressure, $\boldsymbol{g}$ is the gravitational acceleration, σ is the surface tension at the liquid-gas interface, and κ is twice the mean interface curvature. The integral term in equation (4) accounts for surface tension acting on the interface. In order to limit the scope of our study, we have assumed that the surface tension coefficient is constant and thus, without loss of generality, we ignore tangential variations in σ along the interface. We have also assumed the light fluid (chamber cavity gas) to be inviscid, so that the viscosity ratio defined in Equation 5 is equal to zero.

The selected definitions for the length and velocity scales make the Weber number a function of only the density ratio (Equation 8); a density ratio of 20 corresponds to a Weber number of 1.053, while an infinite density ratio corresponds to a Weber number of unity. Values of the length, velocity, and time scales, along with the Reynolds number for several fluids at different temperatures are given in Table I. For chamber designs of interest, the length scale values for these materials result in non-dimensional film thickness of the order of unity. Detailed discussion of the numerical integration scheme used in this investigation may be found in (19).

NUMERICAL RESULTS

Figure 1 shows the flow domain geometry and boundary conditions used to model horizontal, downward facing, surfaces with liquid injection through the surface. This corresponds to the uppermost point in the chamber inner surface. Because of symmetry, periodic boundary conditions are used in the horizontal directions (across the four vertical sides). Liquid is injected at a specified normal velocity at the upper solid boundary, while an open boundary condition is used at the bottom surface. Using the above definition for the velocity scale, U_o, the non-dimensional injection velocity is given by:

$$w_{in}^{*} = \frac{w_{in}}{\left[g\sigma/(\rho_L - \rho_G)\right]^{1/4}} \tag{9}$$

The analysis assumes a uniform injection velocity through the surface; the validity of this assumption will depend on the nature of the porous wall and its wettability by the injected liquid.

The box dimensions in the *x* and *y* directions have been selected to be at least ten times the length scale *l*, while different heights are used (typically 20 to 50 times the length scale) to accommodate liquid penetration into the chamber gas (the light fluid) prior to liquid droplet detachment. The calculation geometry and boundary conditions used to model inclined downward facing surfaces differs from that in Fig. 1, since the symmetry boundary condition across the four side boundaries does not apply. Instead, we have imposed Neumann conditions on the boundary for velocity; the pressure gradients in the *x* and *y* directions are equal to ρg_x and ρg_y, respectively, where g_x and g_y are the gravitational acceleration components. The box is oriented so that gravity acts only in the *x* and *z* directions, i.e. the box is tilted only in the *x* direction with an angle θ from the horizontal.

The effect of surface perturbation geometry and mode number on the evolution of the free surface and the droplet detachment time has been examined. Clearly, in the relatively hostile environment following target explosion, the initial film surface geometry would be highly uncertain. Hence, three different initial surface perturbation geometries have been examined; these are referred to as the "sinusoidal," "random," and "saddle" perturbations (Fig. 2).

For mode number one, the perturbation wavelength is equal to the box size in the *x* and *y* directions. Generally, equal values of film thickness and initial perturbation amplitude have been used in the simulations. For the random initial surface perturbation, an upper bound is imposed on the difference between the maximum and minimum initial film thickness, while the total

initial liquid volume is kept the same as the other two surface perturbations. Typical results showing the effect of initial perturbation geometry on the evolution of the film surface contour and the droplet detachment time are shown in Fig. 3; these results correspond to liquid lead at 700 K with a liquid injection velocity of 1 mm/s. The results generally show that the "saddle" type initial surface perturbation produces the shortest droplet detachment time. Also, within the accuracy of the calculations, the droplet detachment times for the "sinusoidal" perturbation are nearly equal to those for the saddle perturbation. The calculations have been performed with a nodal resolution of (50×50×50). The sensitivity of the results to the nodal resolution has been examined; a finer 100×100×100) mesh results in nearly identical droplet detachment times. The "saddle" perturbation geometry has traditionally been used in previous studies of the Rayleigh-Taylor instability (see for example 20-22). It has therefore been used in the parametric calculations to generate the generalized non-dimensional charts described below.

The random initial surface perturbation is, in essence, equivalent to higher mode number perturbations. The effect of disturbance mode number (i.e. wavelength) on the evolution of the free surface contours and droplet detachment time has been investigated. As expected, the results for the high mode numbers show that the perturbations interact with each other and delay the detachment time of the drop. This result is consistent with the behavior observed in Fig. 3 for a random surface perturbation. Therefore, the generalized non-dimensional charts presented below have been produced using the long wavelength (mode number 1) initial surface perturbations.

As discussed earlier, the selected definitions for the length and velocity scales make the Weber number a function of only the density ratio. Parametric calculations have been performed to quantify the effect of the density ratio (i.e. Weber number) on the evolution of the free surface geometry (19). The results show that beyond a density ratio of approximately 20 (i.e. a Weber

number less than 1.053), the results are insensitive to further increases in the density ratio (i.e. further reductions in the Weber number). Clearly, for IFE applications, the density ratio between the film liquid and the chamber gas will be several orders of magnitude higher than twenty. However, the parametric results referenced above demonstrate that for such applications, the effect of density ratio can be ignored. Therefore, in order to limit the computing time required for the analyses, the generalized non-dimensional charts presented below have been produced using a density ratio of twenty (i.e. a Weber number of 1.053). The remaining non-dimensional parameters are the Reynolds number, the non-dimensional injection velocity (Equation 9), and initial surface geometry.

The effects of liquid injection velocity on the free surface evolution and drop detachment time for a thin (0.2 mm) and a thick (1.0 mm) film are shown in Figs. 4 and 5, respectively. Again, the liquid is assumed to be lead at 700 K, while the injection velocities ranged from zero to 10 mm/s. These results indicate that higher liquid injection velocities tend to accelerate droplet detachment for initially thin liquid films, while the opposite occurs for initially thick films.

The effect of surface inclination angle (0, 5 and 10 degrees) on the evolution of the free surface and droplet detachment is shown in Fig. 6. A longer box is used in the inclined surface cases in order to capture the entire surface evolution prior to droplet detachment. Again, lead at 700 K is the injected liquid, with an initial film thickness of 0.5 mm and an injection velocity of 1.0 mm/s — typical parameters for the Prometheus-L design (11). Droplet detachment is delayed as the inclination angle increases. The generalized charts presented below have, therefore, been developed for the most conservative case, namely a horizontal surface.

Typical results showing variation of the minimum film thickness with non-dimensional time during disturbance growth up to the point of droplet detachment are shown in Fig. 7. The

results show that the film thickness gradually increases with injection, then decreases to a minimum value prior to droplet separation. For initially thin film (Fig 7a), the minimum film thickness is actually higher than the minimum initial value. The opposite is true for initially thick films as shown in Fig. 7b. Recognizing the importance of this parameter to system designers, generalized non-dimensional charts for the minimum film thickness as a function of the initial film thickness, injection velocity and Reynolds number have been developed (see Fig. 8). These results suggest that a minimum injection velocity will be required to prevent the film thickness from decreasing below a designer-specified minimum value.

Parametric calculations have been performed to generate generalized non-dimensional charts for the droplet detachment time (Fig. 9) and equivalent detached droplet diameter (Fig. 10). These results suggest that for thin films, the Reynolds number and injection velocity will significantly impact the droplet detachment time. However, for a non-dimensional initial thickness of 0.5 and greater (approximately $\geq$1 mm for lead at 700 K), the droplet detachment time will be independent of both the Reynolds number and injection velocity. Additionally, for a non-dimensional injection velocity exceeding 0.01 (approximately 1.4 mm/s for lead at 700 K), the detachment time will be nearly independent of the Reynolds number and will depend only on the initial film thickness. These results suggest that liquid film stability may impose a limit on the minimum repetition rate in order to avoid liquid "dripping" into the chamber between shots.

The non-dimensional detached droplet diameter shown in Fig. 10 represents the diameter of a spherical droplet with volume equal to that of the separated spike from the liquid film at the instant of separation. These results suggest that the detached droplet diameter depends weakly on the Reynolds number, and is highly dependent on both the injection velocity and initial film

thickness. The results given in Fig. 10 allow the designer to estimate the size of detached droplets from the liquid film for different design parameters and liquid properties.

EXPERIMENTAL APPARATUS AND RESULTS

Referring to Table 1, the Reynolds number for water at room temperature (~500) falls within the range of interest for most IFE reactor coolants. Hence, experiments using water as a simulant can provide useful data to validate the model described in the previous section. An experimental test facility has been constructed (Figure 11), where water from a constant-head tank is allowed to flow continuously through a porous SS 304 rectangular plate with an adjustable orientation angle. The plate dimensions (~12 × 18 cm) are considerably larger than the characteristic length scale (see Table 1), and are therefore expected to adequately model the behavior of much larger surfaces. Different plate porosities and supply tank levels are used to produce wide ranges of injection velocity and film thickness.

Typical results showing the evolution of a liquid water droplet from a horizontal surface are shown in Figure 12. Preliminary data for the droplet detachment time from a horizontal surface with an injection velocity of 2.4 mm/s are shown in Figure 13. These data represent the distribution of measured values for forty different droplets; the mean droplet detachment time is 0.39 seconds, while the standard deviation among the experimental measurements is 0.04 seconds. The distribution of droplet detachment times is a direct result of the random nature of surface perturbations in the preliminary experiments conducted so far. The mean detached droplet diameter among those examined in Figure 13 is 5.79 mm with a standard deviation of 0.77 mm. Based on an estimated film thickness of 1.0 mm, these results compare well with the model-predicted values of departure time (0.36 sec) and departure diameter (5.5 mm). Precise

measurement of the initial film thickness is necessary in order to provide a more accurate comparison with model predictions. Ultrasound sensors will be used to determine the transient variation of the effective film thickness at different locations on the plate surface.

CONCLUDING REMARKS

A numerical and experimental investigation has been performed to analyze the fluid dynamic aspects of the porous wetted wall protection scheme for IFE reactor first walls. The model extends earlier work on the Rayleigh-Taylor instability by including the effect of a bounding wall through which the heavier fluid is continuously injected. Attention has been focused on the later stages of the instability which lead to droplet detachment. The effects of film thickness, liquid injection velocity, inclination angle, liquid properties, and surface disturbance configuration and amplitude on liquid film stability between target explosions have been examined. The results suggest that liquid film stability may impose a lower limit on the minimum repetition rate in order to avoid liquid "dripping" into the chamber between shots. The results also suggest that a minimum injection velocity is required in order to maintain the film thickness over the entire surface above a specified minimum value to assure adequate wall protection from subsequent shots. The generalized charts presented in Figs. 8-10 make it possible for system designers to establish "design windows" for successful implementation of the wetted wall protection scheme with various coolants and operating conditions.

A preliminary experimental investigation aimed at validating the model has been performed. It is shown that water can be used as a simulant to adequately validate the model over the parameter ranges of interest. Preliminary data show reasonably good agreement between the experiment and model predictions. Extensive comparison between the model and

the experiments will be performed after successful confirmation of transient film thickness measurements at different points on the surface.

REFERENCES

1. S. I. ABDEL-KHALIK AND T. O. HUNTER, "Assessment of Surface Heating Problems in Laser Fusion Reactors", *ASME J. Heat Transfer* **100**, 311 (1978).

2. R.R. PETERSON, "Response of National Ignition Facility First Wall Materials to Target X-rays and Debris", *Fusion Technology* **30**, 778 (1996).

3. R. R. PETERSON, D. A. HAYNES, JR., I. E. GOLOVKIN, and G. A. MOSES, "Inertial Fusion Energy Target Output and Chamber Response: Calculations and Experiments", *Physics of Plasmas*, **9, 2287** (2002).

4. A. R. RAFFRAY, D. A. HAYNES, JR., and F. NAJMABADI, "IFE Chamber Walls: Requirements, Design Options, and Synergy with MFE Plasma Facing Components", *Presented at PSI-15 Meeting, Gifu, Japan* (2002); submitted for publication in Journal of Nuclear Materials.

5. P. F. PETERSON and J. M. SCOTT, "The Mini-Chamber, an Advanced Protection Concept for NIF", *Fusion Technology* **30**, 442 (1996).

6. U. VON MÖLLENDORFF, M.T. TOBIN, "Conceptual Design Considerations for the Reaction Chamber of a Heavy Ion Driven Inertial Fusion Test Facility", *Forschungszentrum Karlsruhe, Technik und Umwelt*, INR 1945 (July 1996).

7. G. L. KULCINSKI, R. R. PETERSON, L. J. WITTENBERG, E. A MOGAHED and I. N. SVIATOSLAVSKY, "Dry Wall Issues for the SOMBRERO Laser Fusion Power Plant", *Fusion Engineering and Design* **60**, 3 (2002).

8. A. HASSANEIN and S. I. ABDEL-KHALIK, "Interaction of Target Debris with Liquid-Film-Protected First Walls", *Presented at ARIES project Meeting, San Diego, CA* (January 2002).

9. L. A. BOOTH, COMPILER, "Central Station Power Generation by Laser-Driven Fusion", LA-4858-MS, *Los Alamos Scientific Laboratory report* (1972).

10. J. M. WILLIAMS, et al., "A Conceptual Laser Controlled Thermonuclear Reactor Power Plant," *Proceedings First Topical Meeting Technology of Controlled Fusion, San Diego, CA* (1974).

11. L. M. WAGANER, et al., "Inertial Fusion Energy Reactor Design Studies", *McDonnell Douglas Report*, DOE/ER-4101, MDC 92E0008, Volume III (March 1992).

12. A. HASSANEIN and I. K. KONKASHBAEV, "Modeling and Simulation of Fragmentation of Suddenly Heated Liquid Metal Jets", *Argonne National Laboratory Report*, ANL-ET/01-13 (June 2001).

13. R. L. ENGELSTAD, "Vibration and Stability of Vertical Tubes Conveying Fluid Subjected to Planar Excitation", *PhD Thesis*, University of Wisconsin-Madison (1988).

14. M. S. EL-GENK and H. H. SABER, "Minimum Thickness of a Flowing Down Liquid Film on a Vertical Surface", *Int. J. Heat Mass Transfer* **44**, 2809 (2001).

15. D. E. HARTLEY and W. MURGATROY, "Criteria for the Break-up of Thin Liquid Layers Flowing Isothermally over a Solid Surface", *Int. J. Heat Mass Transfer* **7**, 1003 (1964).

16. S. G. BANKOFF, "Minimum Thickness of a Draining Liquid Film", *Int. J. Heat Mass Transfer* **14**, 2143 (1971).

17. J. MIKIELEWICZ and J. R. MOSZYNSKI, "Minimum Thickness of a Liquid Film Flowing Vertically Down a Solid Surface", *Int. J. Heat Mass Transfer* **19**, 771 (1976).

18. A. DONIEC, "Laminar Flow of a Liquid Rivulet Down a Vertical Solid Surface", *Canadian J. Chem. Eng.* **69**, 198 (1991).

19. S. SHIN, "A Level Contour Reconstruction Method for Three-Dimensional Multiphase Flows and Its Application", *Ph.D. Thesis*, Georgia Institute of Technology (2002).

20. G. TRYGGVASON and S.O. UNVERDI, "Computations of Three-Dimensional Rayleigh-Taylor Instability", *Phys. Fluids A.* **2**, 656 (1990).

21. S. O. UNVERDI and G. TRYGGVASON, "A Front-Tracking Method for Viscous, Incompressible, Multi-Fluid Flows", *J. Comput. Phys.* **100**, 25 (1992).

22. S. O. UNVERDI and G. TRYGGVASON, "Computations of Multi-Fluid Flows", *Physica D.* **60**, 70 (1992).

23. S. SHIN and D. JURIC, "Modeling Three-Dimensional Multiphase Flow Using a Level Contour Reconstruction Method for Front Tracking Without Connectivity", *J. Comput. Phys.* (2002), **180**, 427 (2002).

ACKNOWLEDGMENT

This work was performed in support of the ARIES-IFE project. Numerous discussions with members of the ARIES project team are gratefully acknowledged. Financial support was provided in part by the U.S. Department of Energy through contract # DE-FG02-01ER54656.

NOMENCLATURE

$I(\mathbf{x},t)$ indicator function

$\mathbf{n}$ unit normal to the interface

$\mathbf{x}_f$ parameterization of the interface

$\delta(\mathbf{x}-\mathbf{x}_f)$ three-dimensional delta function

$\mathbf{V}$ interface velocity vector.

l length scale, $(\leftarrow/g(\rightarrow_L-\rightarrow_G))^{1/2}$

U_o velocity scale, $(gl)^{1/2}$

P_o pressure scale, $\rightarrow_L U_o^2$

t_o time scale, l/U_o

P pressure

$\boldsymbol{g}$ gravitational acceleration

z_o^* nondimensional initial surface thickness measured from the top

L_x^* nondimensional box dimensions in the y directions

L_y^* nondimensional box dimensions in the y directions

Re Reynolds number, $\rho_L U_o l / \mu_L$

We Weber number, $\rho_L U_o^2 l / \sigma = \rho_L / (\rho_L - \rho_G)$

Greek Letters

$\odot_s^*$ nondimensional perturbation amplitude

ρ density

μ viscosity

ρ^* density ratio, ρ_G / ρ_L

μ^* viscosity ratio, μ_G / μ_L

σ surface tension coefficient

κ twice the mean interface curvature

subscripts

L film liquid injected through the porous wall (heavy fluid)

G low pressure gas (vacuum) within the chamber (light fluid)

Table I

Values of the scaling length, velocity, and time, along with the

Reynolds number for Various Coolants

	Water		**Lead**		**Lithium**		**Flibe**		
***T*(K)**	**20°C**	**50°C**	**700 K**	**800 K**	**523 K**	**723 K**	**773 K**	**873 K**	**973 K**
***l* (mm)**	2.73	2.65	2.14	2.12	8.25	7.99	3.35	3.22	3.17
U_o (mm/s)	163.5	161.2	144.7	144.2	284.4	280.0	181.4	177.8	176.4
t_o (ms)	16.7	16.4	14.8	14.7	29.0	28.6	18.5	18.1	18.0
Re	445	771.2	1618	1831	1546	1775	81.80	130.8	195.3

FIGURE CAPTIONS

Fig. 1: Initial surface configuration and boundary conditions used to model horizontal, downward-facing, surfaces with liquid injection through the surface.

Fig. 2: Schematic diagram of the three initial surface perturbation geometries examined in this investigation.

Fig. 3: Effect of initial surface perturbation geometry on the evolution of the free surface for liquid lead at 700 K [Box size = 50×50×50 mm; injection velocity = 1 mm/s; nodal resolution = 50×50×50; indicated droplet detachment times are in seconds].

Fig. 4: Effect of liquid injection velocity on droplet detachment time and evolution of the free surface for liquid lead at 700K with an initial liquid film thickness of 0.2 mm. [Box size = 50×50×50 mm; nodal resolution = 50×50×50].

Fig. 5: Effect of liquid injection velocity on droplet detachment time and evolution of the free surface for liquid lead at 700K with an initial liquid film thickness of 1.0 mm. [Box size = 50×50×50 mm; nodal resolution = 50×50×50].

Fig. 6: Effect of inclination angle on droplet detachment time and evolution of the free surface for liquid lead at 700K with an initial film thickness of 0.5 mm and injection velocity of 1.0 mm/s.

Fig. 7: Transient variation of the non-dimensional minimum film thickness prior to droplet detachment. (a) Thin film ($z_o^* = 0.1$). (b) Thick film ($z_o^* = 0.5$).

Fig. 8: Generalized non-dimensional charts for the minimum film thickness during the transient. (a) Thin film ($z_o^* = 0.1$). (b) Intermediate film ($z_o^* = 0.2$). (c) Thick film ($z_o^* = 0.5$).

Fig. 9: Generalized non-dimensional charts for the non-dimensional droplet detachment time as a function of injection velocity and Reynolds number for different film thickness. (a) Thin film ($z_o^* = 0.1$). (b) Intermediate film ($z_o^* = 0.2$). (c) Thick film ($z_o^* = 0.5$).

Fig. 10: Generalized non-dimensional charts for the non-dimensional detached droplet diameter as a function of injection velocity and Reynolds number for different film thickness. (a) Thin film ($z_o^* = 0.1$). (b) Intermediate film ($z_o^* = 0.2$). (c) Thick film ($z_o^* = 0.5$).

Fig. 11: Schematic Diagram of the Experimental Apparatus

Fig. 12: Photographs of liquid water droplet growth for a 10 mm/s injection velocity.

Fig. 13: Experimental data for distribution of droplet detachment times ($w_{in} = 2.4$ mm/s)

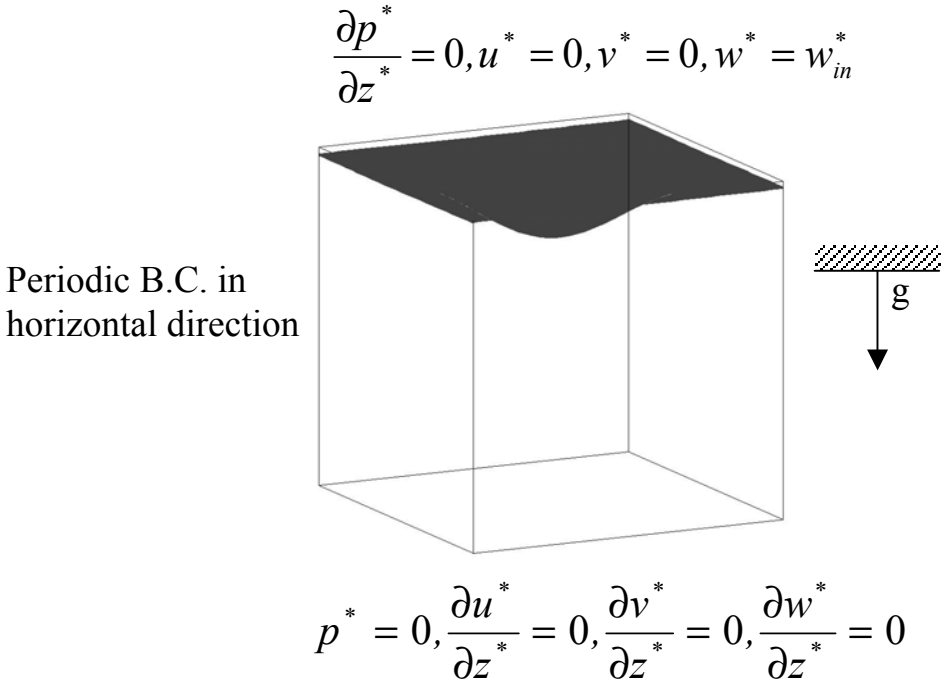

Manuscript # : 269702
Manuscript title : Fluid Dynamic Aspects of the Porous Wetted Wall Protection Scheme for IFE Reactors
Authors : S. Shin, F. Abdelall, D. Juric, S. I. Abdel-Khalik, M. Yoda, D. Sadowski, and the ARIES Team
Fig. 1

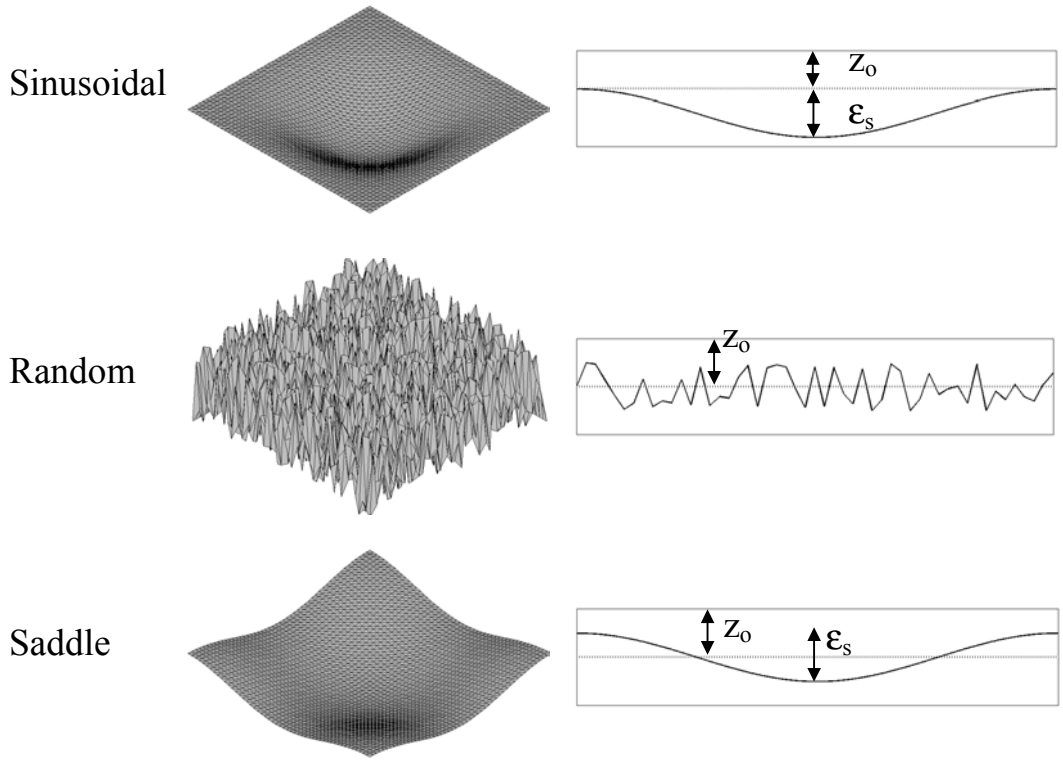

Manuscript # : 269702
Manuscript title : Fluid Dynamic Aspects of the Porous Wetted Wall Protection Scheme for IFE Reactors
Authors : S. Shin, F. Abdelall, D. Juric, S. I. Abdel-Khalik, M. Yoda, D. Sadowski, and the ARIES Team
Fig. 2

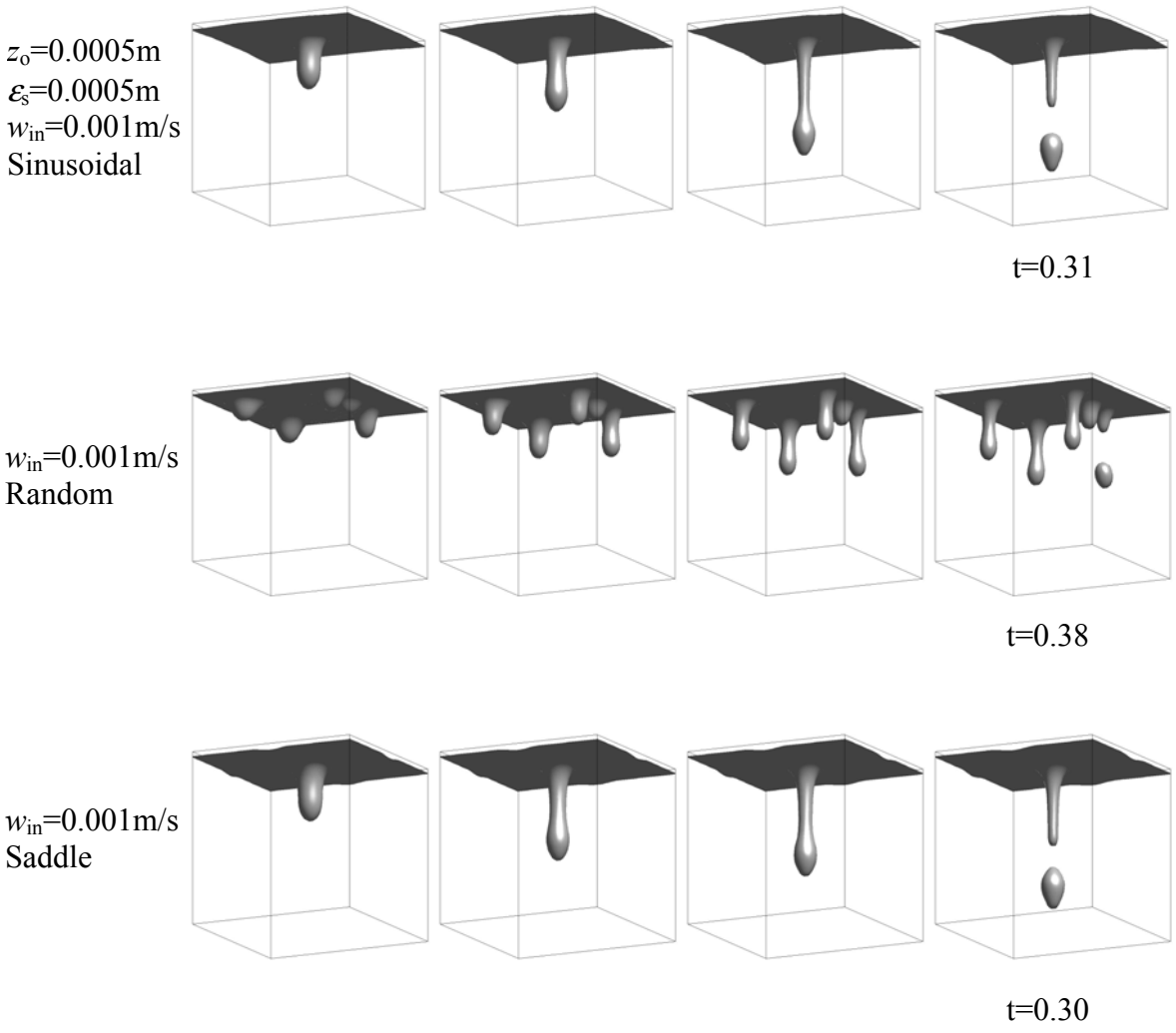

Manuscript # : 269702
Manuscript title : Fluid Dynamic Aspects of the Porous Wetted Wall Protection Scheme for IFE Reactors
Authors : S. Shin, F. Abdelall, D. Juric, S. I. Abdel-Khalik, M. Yoda, D. Sadowski, and the ARIES Team
Fig. 3

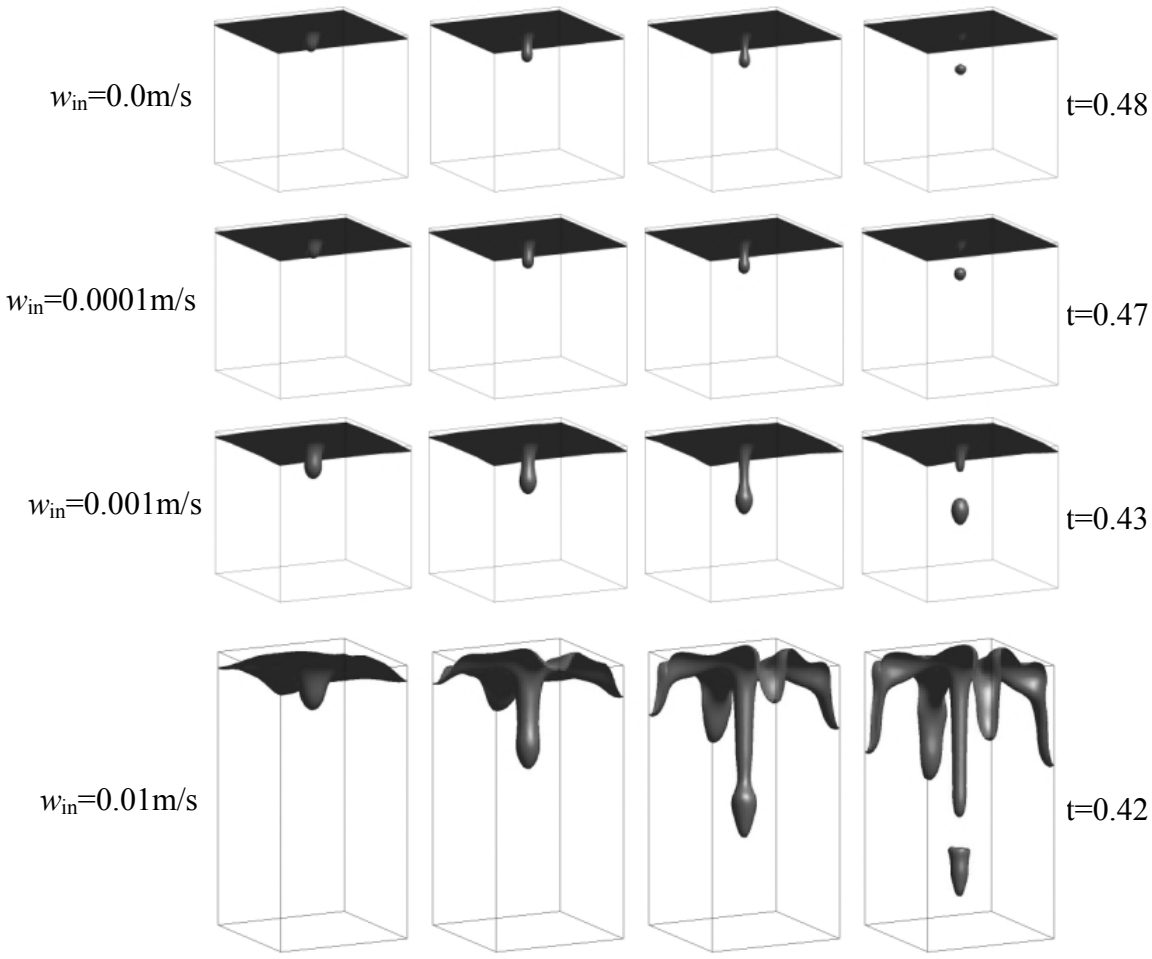

Manuscript # : 269702
Manuscript title : Fluid Dynamic Aspects of the Porous Wetted Wall Protection Scheme for IFE Reactors
Authors : S. Shin, F. Abdelall, D. Juric, S. I. Abdel-Khalik, M. Yoda, D. Sadowski, and the ARIES Team
Fig. 4

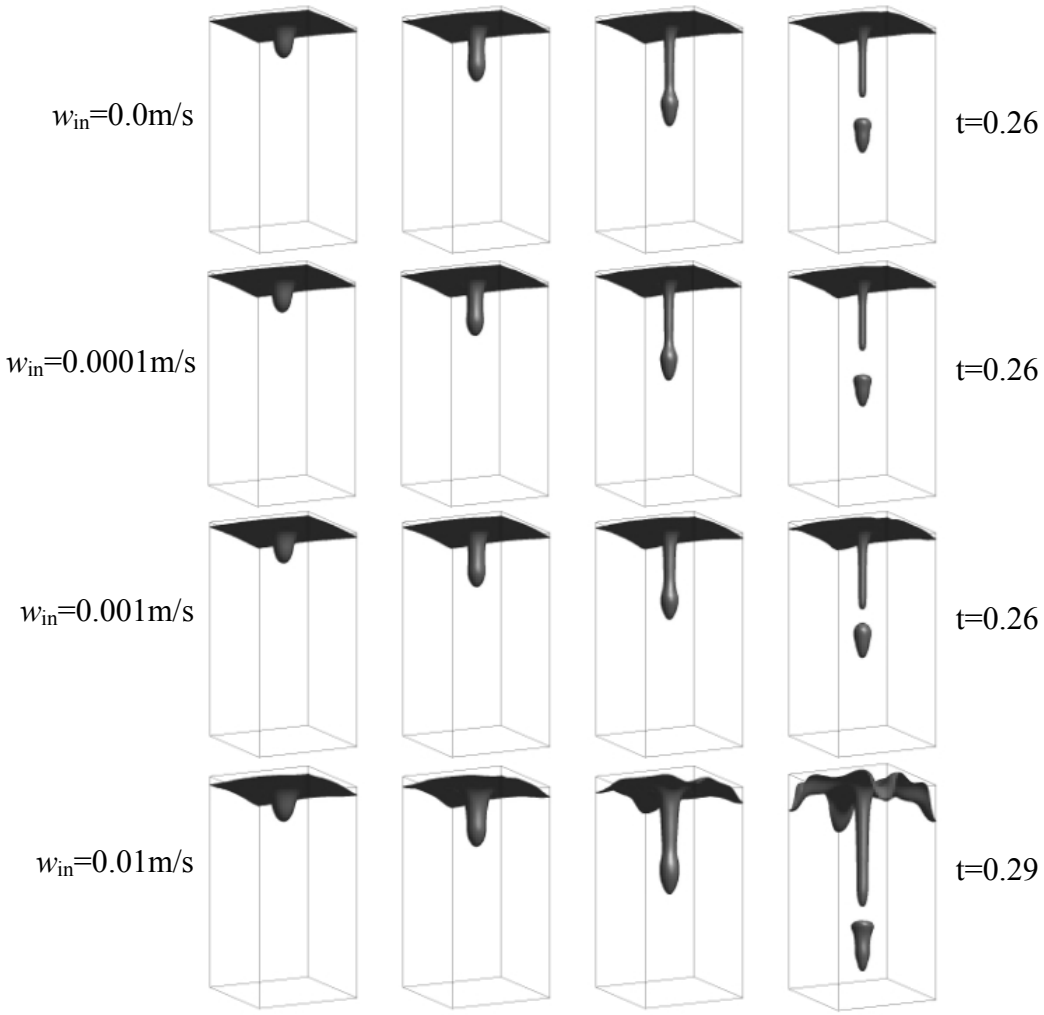

Manuscript # : 269702
Manuscript title : Fluid Dynamic Aspects of the Porous Wetted Wall Protection Scheme for IFE Reactors
Authors : S. Shin, F. Abdelall, D. Juric, S. I. Abdel-Khalik, M. Yoda, D. Sadowski, and the ARIES Team
Fig. 5

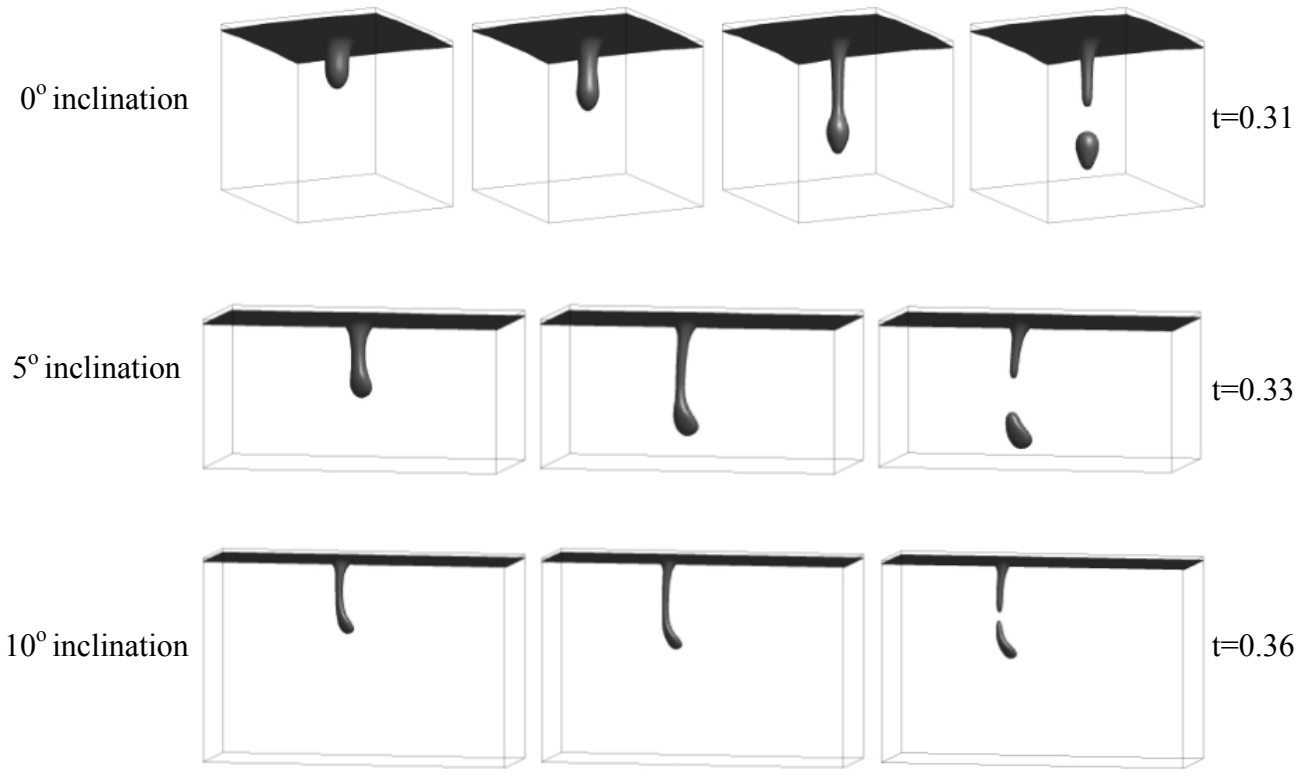

Manuscript # : 269702
Manuscript title : Fluid Dynamic Aspects of the Porous Wetted Wall Protection Scheme for IFE Reactors
Authors : S. Shin, F. Abdelall, D. Juric, S. I. Abdel-Khalik, M. Yoda, D. Sadowski, and the ARIES Team
Fig. 6

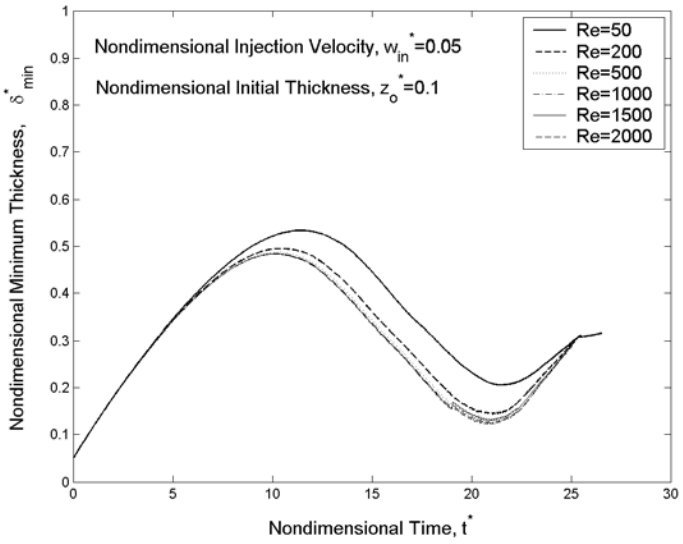

(a)

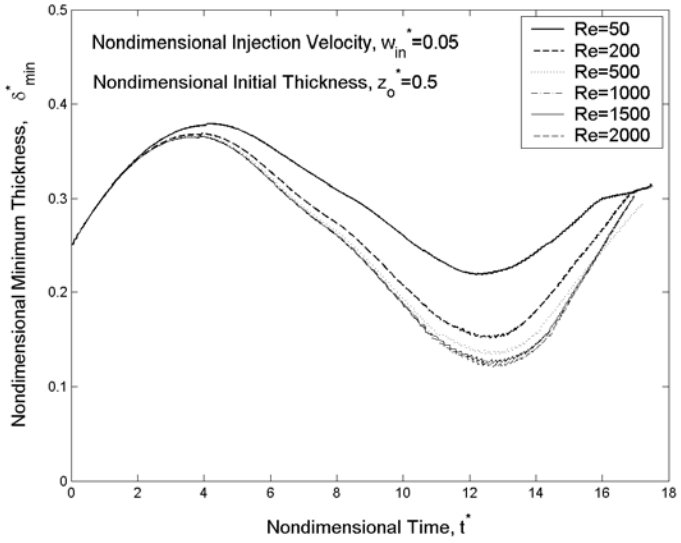

(b)

Manuscript # : 269702
Manuscript title : Fluid Dynamic Aspects of the Porous Wetted Wall Protection Scheme for IFE Reactors
Authors : S. Shin, F. Abdelall, D. Juric, S. I. Abdel-Khalik, M. Yoda, D. Sadowski, and the ARIES Team
Fig. 7

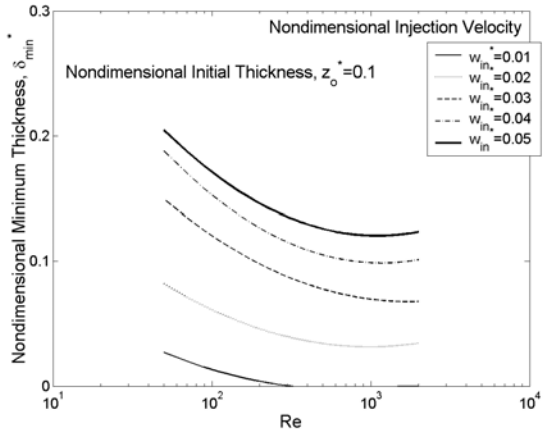

(a)

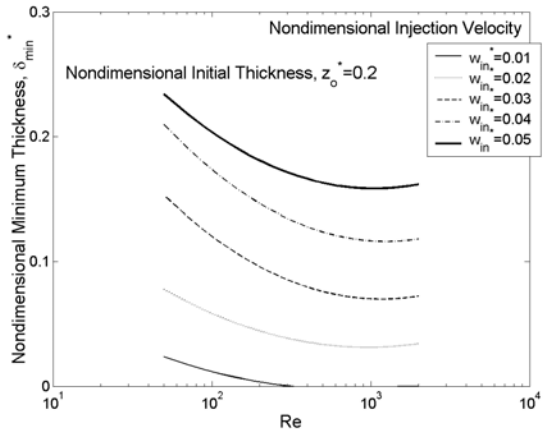

(b)

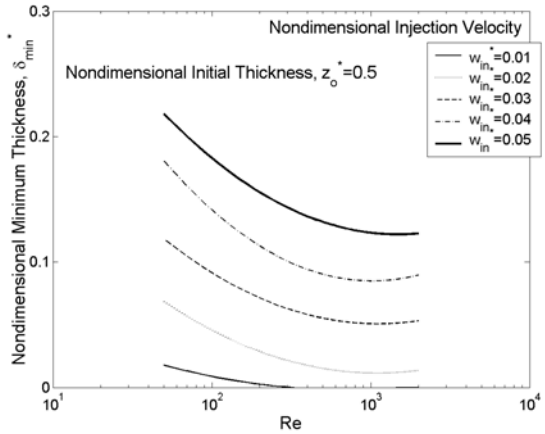

(c)

Manuscript # : 269702
Manuscript title : Fluid Dynamic Aspects of the Porous Wetted Wall Protection Scheme for IFE Reactors
Authors : S. Shin, F. Abdelall, D. Juric, S. I. Abdel-Khalik, M. Yoda, D. Sadowski, and the ARIES Team
Fig. 8

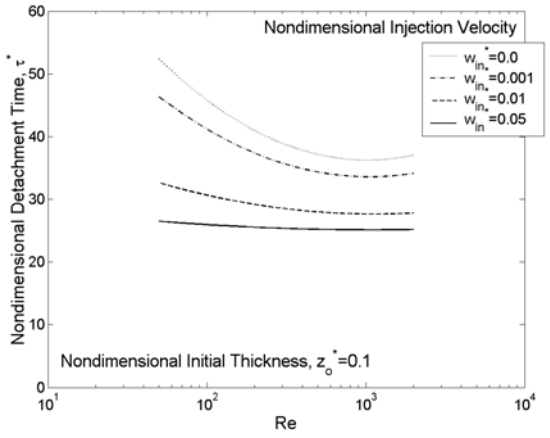

(a)

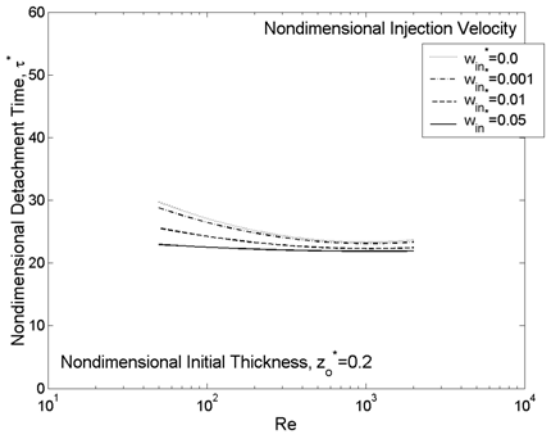

(b)

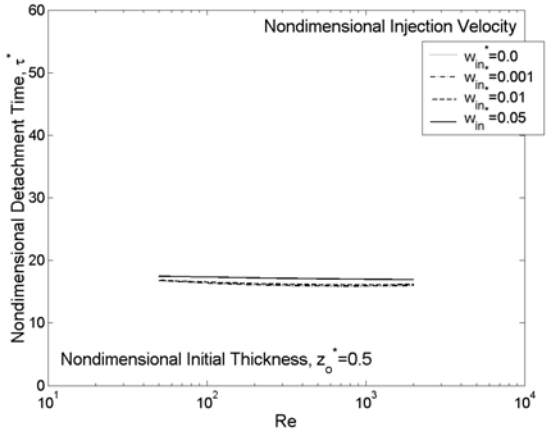

(c)

Manuscript # : 269702
Manuscript title : Fluid Dynamic Aspects of the Porous Wetted Wall Protection Scheme for IFE Reactors
Authors : S. Shin, F. Abdelall, D. Juric, S. I. Abdel-Khalik, M. Yoda, D. Sadowski, and the ARIES Team
Fig. 9

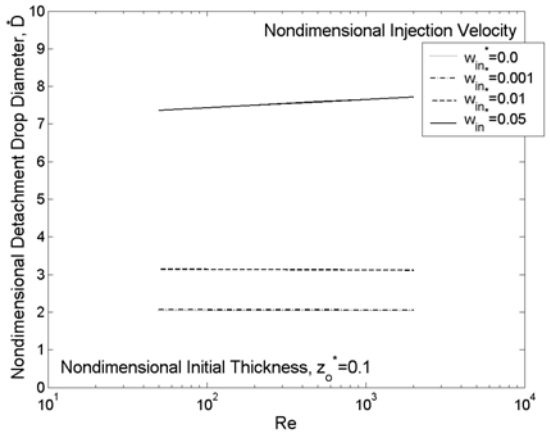

(a)

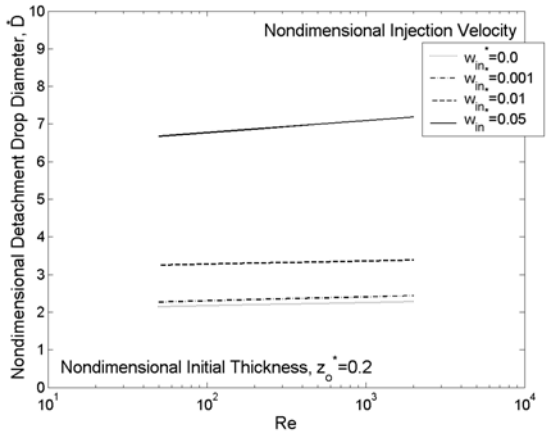

(b)

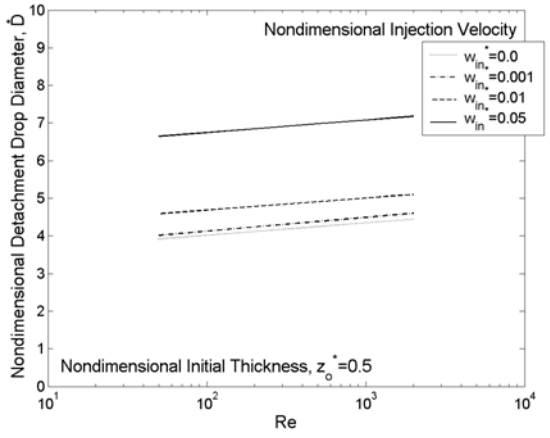

(c)

Manuscript # : 269702
Manuscript title : Fluid Dynamic Aspects of the Porous Wetted Wall Protection Scheme for IFE Reactors
Authors : S. Shin, F. Abdelall, D. Juric, S. I. Abdel-Khalik, M. Yoda, D. Sadowski, and the ARIES Team
Fig. 10

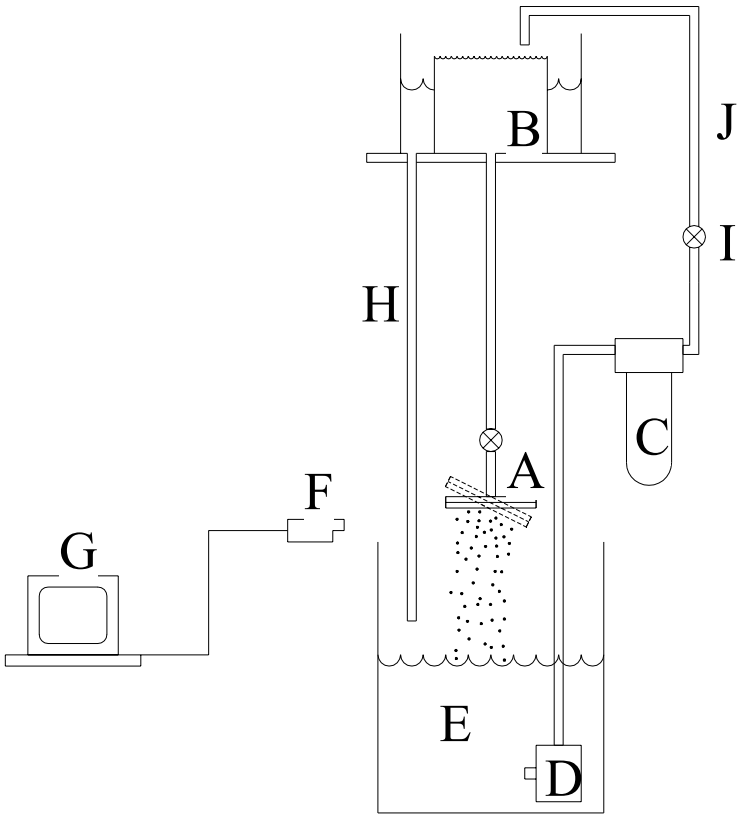

A Porous plate holder w/adjustable orientation
B Constant-head plenum w/adjustable height
C Sub-micron filter
D Sump pump
E Reservoir
F CCD camera
G Data acquisition computer
H Plenum overflow line
I Flow metering valve
J Flexible tubing

Manuscript # : 269702
Manuscript title : Fluid Dynamic Aspects of the Porous Wetted Wall Protection Scheme for IFE Reactors
Authors : S. Shin, F. Abdelall, D. Juric, S. I. Abdel-Khalik, M. Yoda, D. Sadowski, and the ARIES Team
Fig. 11

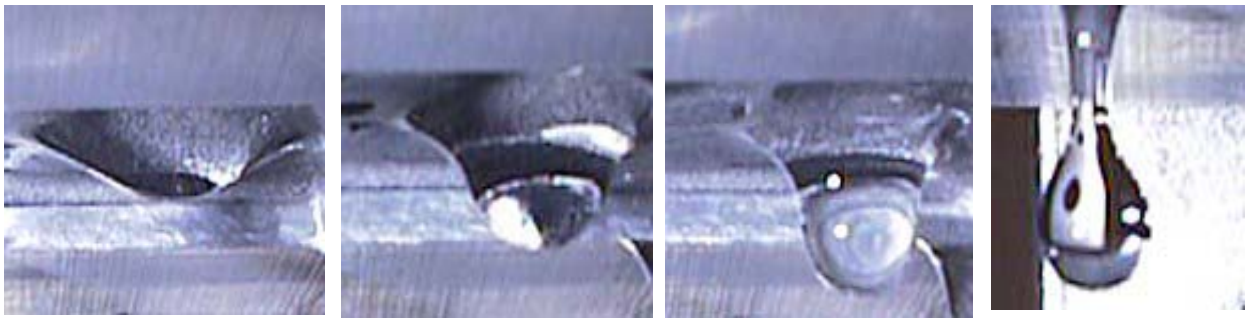

0.05 s 0.15 s 0.2 s

Injection velocity w_{in} = 10 mm/sec

Manuscript # : 269702
Manuscript title : Fluid Dynamic Aspects of the Porous Wetted Wall Protection Scheme for IFE Reactors
Authors : S. Shin, F. Abdelall, D. Juric, S. I. Abdel-Khalik, M. Yoda, D. Sadowski, and the ARIES Team
Fig. 12

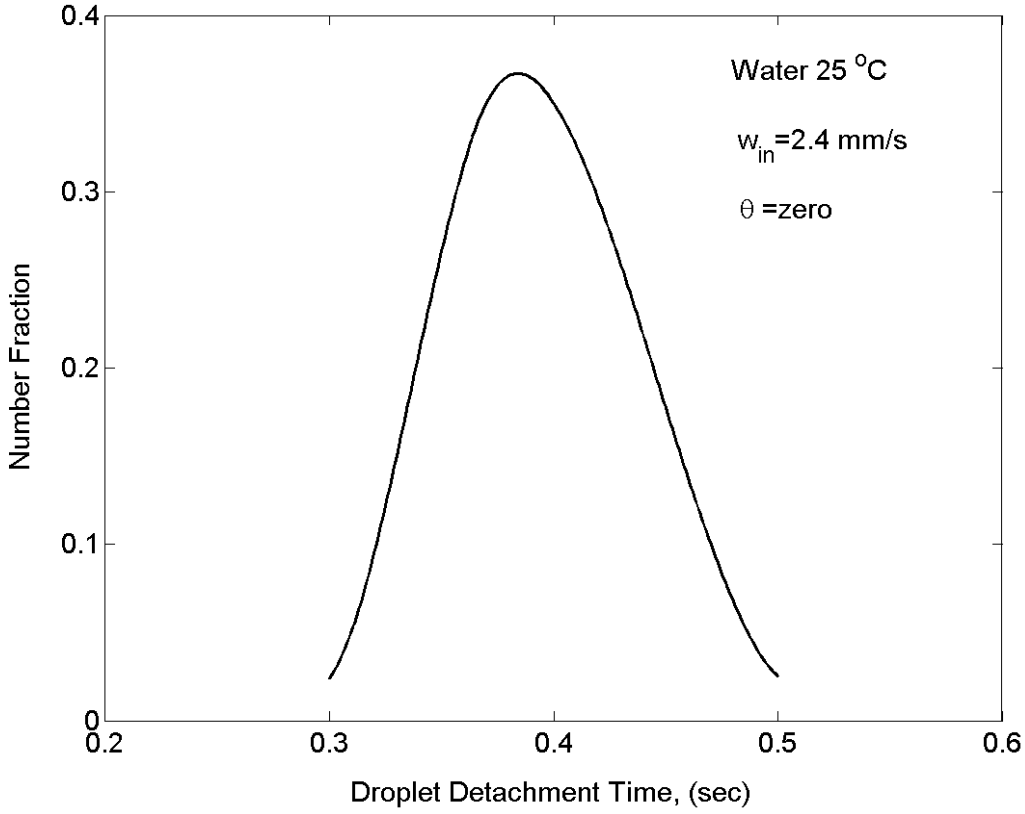

Manuscript # : 269702
Manuscript title : Fluid Dynamic Aspects of the Porous Wetted Wall Protection Scheme for IFE Reactors
Authors : S. Shin, F. Abdelall, D. Juric, S. I. Abdel-Khalik, M. Yoda, D. Sadowski, and the ARIES Team
Fig. 13